Materials Science & Engineering C 123 (2021) 112003

Contents lists available at ScienceDirect

Materials Science & Engineering C

journal homepage: www.elsevier.com/locate/msec

Borax-loaded injectable alginate hydrogels promote muscle regeneration *in vivo* after an injury

Jesús Ciriza [a,b,1], Ana Rodríguez-Romano [a,c,1], Ignacio Nogueroles [c], Gloria Gallego-Ferrer [a,c], Rubén Martín Cabezuelo [c], José Luis Pedraz [a,b], Patricia Rico [a,c,*]

[a] Biomedical Research Networking Center in Bioengineering, Biomaterials and Nanomedicine (CIBER-BBN), Spain
[b] NanoBioCel Group, Laboratory of Pharmacy and Pharmaceutical Technology, Faculty of Pharmacy, University of the Basque Country UPV/EHU, C/ Miguel de Unamuno, 3, 01006 Vitoria Gasteiz, Spain
[c] Center for Biomaterials and Tissue Engineering (CBIT), Universitat Politècnica de València, Camino de Vera s/n, 46022 Valencia, Spain

ARTICLE INFO

Keywords:
Borax
Integrins
Muscle regeneration
NaBC1 transporter (*SLC4A11*)
Alginate hydrogels

ABSTRACT

Muscle tissue possess an innate regenerative potential that involves an extremely complicated and synchronized process on which resident muscle stem cells play a major role: activate after an injury, differentiate and fuse originating new myofibers for muscle repair. Considerable efforts have been made to design new approaches based on material systems to potentiate muscle repair by engineering muscle extracellular matrix and/or including soluble factors/cells in the media, trying to recapitulate the key biophysical and biochemical cues present in the muscle niche. This work proposes a different and simple approach to potentiate muscle regeneration exploiting the interplay between specific cell membrane receptors. The simultaneous stimulation of borate transporter, NaBC1 (encoded by *SLC4A11*gene), and fibronectin-binding integrins induced higher number and size of focal adhesions, major cell spreading and actin stress fibers, strengthening myoblast attachment and providing an enhanced response in terms of myotube fusion and maturation. The stimulated NaBC1 generated an adhesion-driven state through a mechanism that involves simultaneous NaBC1/$\alpha_5\beta_1$/$\alpha_v\beta_3$ co-localization. We engineered and characterized borax-loaded alginate hydrogels for an effective activation of NaBC1 *in vivo*. After inducing an acute injury with cardiotoxin in mice, active-NaBC1 accelerated the muscle regeneration process. Our results put forward a new biomaterial approach for muscle repair.

1. Introduction

Muscle repair is a common adaptive response occurring in many physiological and/or pathological processes such as myopathies. Following injury of adult muscle, quiescent muscle stem cells (satellite cells SCs), activate and re-enter the cell cycle following a complicated and synchronized process of proliferation and differentiation that finally leads to regeneration of injured myofibers [1]. Regeneration process takes place within a short period (21 days in young adult mice) following a considerable crosstalk between endothelial, fibro-adipogenic and myogenic cells to coordinate angiogenesis, connective tissue formation/remodeling and myogenesis [2].

Integrins, the main transmembrane mechanosensors that link extracellular matrix (ECM) to the intracellular cytoskeleton, are bidirectionally regulated by intracellular [3] and extracellular [4] signals giving rise to focal adhesions. In skeletal muscle in particular, β_1 integrin and its partners (α_1, α_3, α_4, α_5, α_6, α_7) [5] regulate myogenic gene expression, migration, fusion, and muscle stability [6] and $\alpha_v\beta_3$participates in regenerating muscle representing an essential component of focal adhesions in myoblast precursor cells and is required for the maintenance of Rac1 activity in differentiated myoblasts promoting myogenesis [7]. Skeletal muscle integrins bind to muscle ECM (including basement membrane), mainly composed of members of the laminin family, fibronectin, proteoglycans and the collagen IV family [8]. Among the basement membrane components, fibronectin is a unique multifunctional protein that rises massively after muscle injury and has an important contribution to support proliferation and differentiation of satellite cells [9–10].

* Corresponding author at: Biomedical Research Networking Center in Bioengineering, Biomaterials and Nanomedicine (CIBER-BBN), Spain.
E-mail addresses: jesus.ciriza@ehu.eu (J. Ciriza), ggallego@ter.upv.es (G. Gallego-Ferrer), rubmarca@doctor.upv.es (R.M. Cabezuelo), joseluis.pedraz@ehu.eus (J.L. Pedraz), parico@upvnet.upv.es (P. Rico).
[1] Equal contribution.

https://doi.org/10.1016/j.msec.2021.112003
Received 30 October 2020; Received in revised form 5 February 2021; Accepted 20 February 2021
Available online 3 March 2021

Besides integrins, ion-channels that control cell homeostasis regulating ion fluxes, act as molecular sensors that can also perceive force after activation by ligand binding, membrane stretch and interaction with other specific ligands or changes in membrane potential [11], so they can communicate extracellular signals to the cytoplasmic environment [12] and integrins [13]. The specific contribution of skeletal muscle ion-channels in muscle is broadly recognized, since extracellular Ca^{2+}, K^{+} and Cl^{-} play an essential role in muscle cell adhesion, muscle development, migration and/or fusion [14], although their precise roles in muscle regeneration are still debated and the information available is restricted to Ca^{2+}, K^{+} and Cl^{-} channels [15].

The NaBC1 (encoded by the *SLC4A11* gene), boron (B) transporter, controls borate homeostasis and functions as an obligated Na^{+}-coupled borate co-transporter [16]. NaBC1 gene mutations cause endothelial corneal dystrophies [17,18]. We have previously reported that borax promotes myogenic differentiation in C2C12 [19], and recently demonstrated a novel function for NaBC1 besides controlling borate homeostasis. We proposed a 3D molecular model for NaBC1 and described that after activation stimulates intracellular signaling promoting vascularization in coordination with growth factor receptors and $\alpha_5\beta_1/\alpha_v\beta_3$ integrins [20]. Further work with Mesenchymal Stem Cells showed that active-NaBC1 enhances cell adhesion determining cellular fate *versus* osteogenic commitment *via* crosstalk of NaBC1, Bone Morphogenetic Protein Receptor 1A (BMPR1A) and $\alpha_5\beta_1/\alpha_v\beta_3$ integrins [21]. Little is known about B homeostasis and function in mammalian cells, and only one report describes the possible role of boric acid in muscle differentiation from adipose-derived stem cells [22]. However, due to the particular chemical properties of B, this metalloid is widely used in medicinal chemistry [23], and several biomaterial-based approaches use B as an intrinsic component of the biomaterial platforms for diverse applications [24,25].

A broad range of biomaterials has been used for skeletal muscle repair comprising ECM derivatives (collagen, fibrin, gelatin), polysaccharides (hyaluronic acid, chitosan, keratin, alginate), decellularized matrices or synthetic biomaterials (PGA, PLA, PLGA) [26–29]. Major strategies for functionalization of biomaterial matrices are based on the delivery of growth factors (GFs) or other small bioactive molecules [30,31]. However, scarce reports describe material systems for ion-delivery to stimulate intracellular signaling [32–35]. Still, there is a need to develop new methods and materials, which promote skeletal muscle repair and functional regeneration.

We have exploited the ability of borax stimulating intracellular signaling for engineering injectable borax-loaded alginate-based hydrogels for promotion of muscle regeneration after injury. To investigate the role of the active-NaBC1 transporter during skeletal muscle regeneration we analyzed *in vitro* muscle C2C12 behavior in terms of cell adhesion, ECM reorganization, cell migration and myotube formation. We observed that active-NaBC1 induces an adhesion-driven state (mature focal adhesions, cell spreading and actin stress fibers) that leads to enhancement of myotube formation. We further demonstrated the role of active-NaBC1 *in vivo*, using a model of cardiotoxin-induced muscle injury. We propose a novel mechanism involving crosstalk and co-localization of active NaBC1/$\alpha_5\beta_1/\alpha_v\beta_3$ integrins and a new function for NaBC1 participating in muscle regeneration besides controlling borate homeostasis.

2. Results

For all the *in vitro* experiments, we have used a murine C2C12 cell line. It is as a model of muscle cellular system, widely used for their rapid proliferation and easy differentiation into myotubes, closely resembling the *in vivo* events participating in skeletal muscle development [36]. We started with the hypothesis that the combined system composed of fibronectin as extracellular matrix (ECM) protein, and borax for NaBC1 transporter stimulation, could enhance muscle regeneration. We based in our previous results, showing that combination of fibronectin and borax-released from a PLLA-based biomaterial system and its interplay with Ca^{2+}, promoted myogenic differentiation in C2C12 cells [19], induced vascularization in human umbilical vein endothelial cells (HUVEC) [20] and drives osteogenesis in Mesenchymal Stem Cells (MSC) [21]. We have used B, in the form of Sodium Tetraborate Decahydrate (borax) dissolved in the culture media for NaBC1 activation, and fibronectin for fibronectin-binding integrin activation.

We first evaluated borax cytotoxicity to assess the range of working concentrations for this muscle cell line, in particular in differentiation conditions, when myotubes are formed, condition that mimic more precisely the environment where muscle regeneration occurs. Fig. S1 shows C2C12 viability, indicating that borax concentrations higher than 52 mM (20 mg mL^{-1}) are toxic for the cells while borax concentrations higher than 15.7 mM (6 mg mL^{-1}) inhibit the formation of myotubes. In all the *in vitro* experiments, we have used borax 0.59 mM, within the 0.2 mg mL^{-1} range, concentration that allow myotube formation and avoid borax experimental toxic effects. We have selected borax 0.59 mM for *in vitro* experimentation based in our previous published results showing that this concentration produces a biological effect in C2C12 cells [19].

2.1. Active-NaBC1 induces muscle C2C12 cell adhesion and fibronectin-binding integrins expression

We have studied the combined effect of NaBC1 and fibronectin-binding integrins stimulation in C2C12 cell adhesion, after 0.5 h, 1 h and 1.5 h of culture. Glass cover slips were used as substrates coated with 20 μg mL^{-1} fibronectin for fibronectin-binding integrin stimulation and 0.59 mM borax dissolved in the culture medium for NaBC1 stimulation (Glass-B). Cells were seeded at low density (5000 cells cm^{-2}) for minimizing cell-cell contacts and in absence of serum for ensuring $\alpha_5\beta_1$ and $\alpha_v\beta_3$ integrins activation. We have previously tested that adsorption of fibronectin is independent of the presence/absence of borax, disregarding ion influence on fibronectin surface density [19].

Fig. 1-a shows C2C12 cell adhesion morphology in Glass control and Glass-B substrates. In all cases, cells exhibited strong actin stress fibers as well as defined focal adhesions revealed by vinculin staining in the different time points. However, focal adhesion sites were more evident in Glass-B substrates. Quantification of cell parameters (Fig. 1-b), shows that circularity decreases at 1.5 h and cell spreading increases with time, as expected. Nevertheless, the presence of borax induced significant differences in the cell spreading area after 1.5 h of culture.

Focal adhesions quantification resulted in a higher total focal adhesions number and larger focal adhesions area in the presence of borax (Fig. 1-b) after 0.5 h, 1 h and 1.5 h, indicative of the enhancement of C2C12 adhesion and its dependence of an active-NaBC1. Focal adhesions size results were similar between Glass and Glass-B after 1 h and 1.5 h of culture, though significant differences were found after 0.5 h of culture in the presence of borax, indicating that active-NaBC1 accelerates focal adhesions maturation in early adhesion stages. Further, cytoskeleton analysis revealed that Glass-B substrate presented significantly higher levels of actin stress fibers at the different time points, suggesting that NaBC1 stimulation responds by increasing cell adhesion. To further prove our hypothesis considering an increased cell adhesion effect after NaBC1 activation, we quantified nuclear morphology. Borax presence reduced nuclear circularity while increased nuclear size and nuclear aspect ratio after 0.5 h, 1 h and 1.5 h of culture (Fig. S2), suggesting that active-NaBC1 induce intracellular tension and nuclear stress altering nuclear morphology.

Integrins are the main cellular receptors mediating cell attachment, and initiate cell adhesion by binding extracellular matrix proteins. This initial binding is quickly followed by integrin binding to the actin cytoskeleton generating a pulling force and recruiting additional adhesion proteins that undergo further maturation originating supramolecular focal adhesions structures [37]. We next examined whether cell adhesion triggered by active-NaBC1 involved alteration of the gene and protein expression of fibronectin-binding integrins. Skeletal muscle ECM

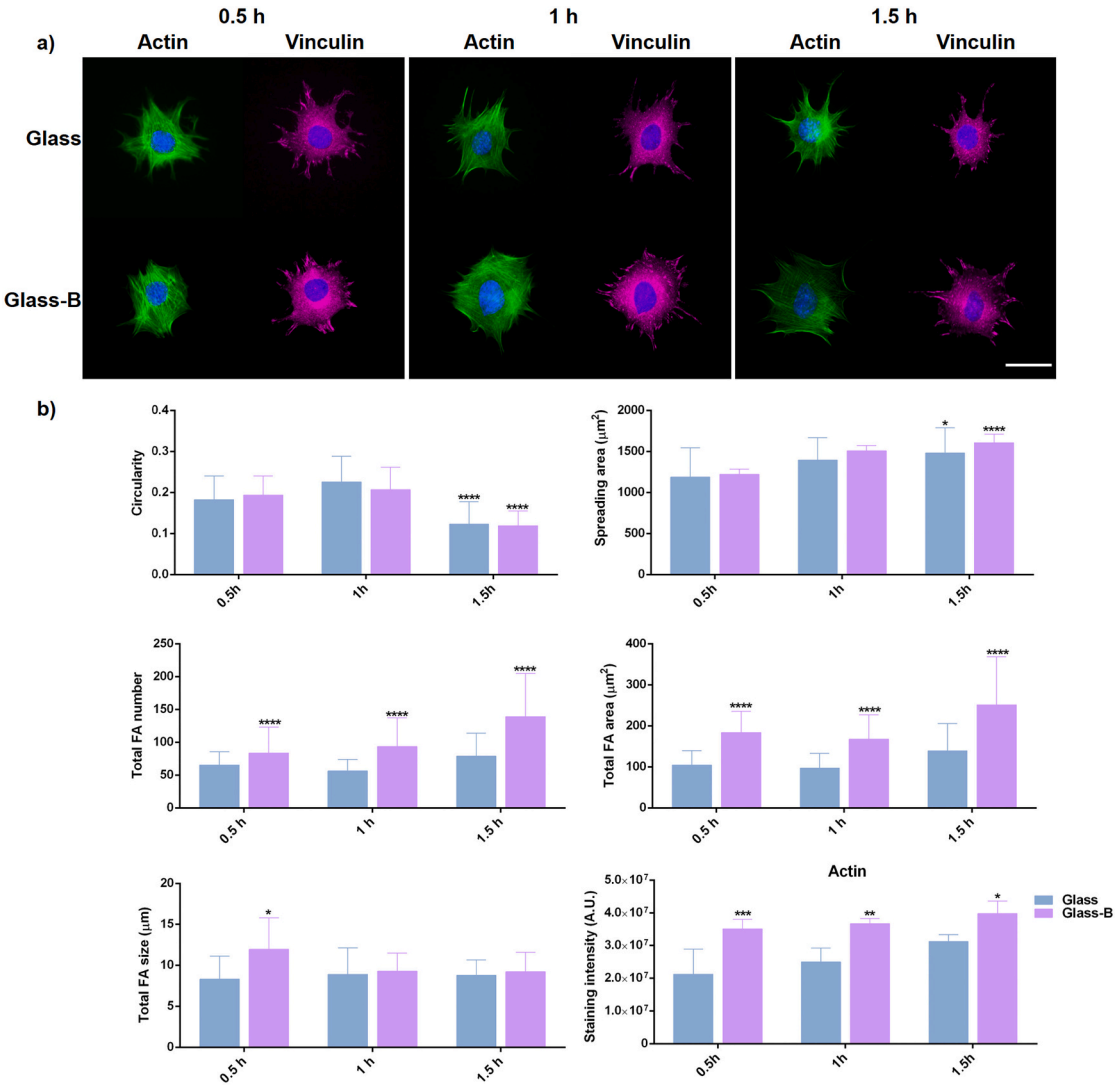

Fig. 1. C2C12 cell adhesion after NaBC1 and fibronectin-binding activation. a) Immunofluorescence images of actin cytoskeleton (green), nuclei (blue) and vinculin (magenta) as a marker of focal adhesions. C2C12 cells were cultured for 0.5, 1 and 1.5 h onto fibronectin-coated glass substrates (Glass), and in the presence of 0.59 mM borax (Glass-B). NaBC1 activation induced clear focal adhesions as a result of vinculin staining at the different time points. Scale bar 50 μm. b) Image analysis quantification of different parameters related to cell shape, spreading area, focal adhesions (FA) and total actin stress fibers. NaBC1 activation induced more focal adhesions number and area after 0.5, 1 and 1.5 h. Bigger focal adhesions are present after NaBC1 activation after 0.5 h of culture. Active-NaBC1 induces actin stress fibers formation at the different time points evaluated. Statistics are shown as mean ± standard deviation. n = 15 images/condition from three different biological replicas. Data were analyzed by an ordinary two-way ANOVA test and corrected for multiple comparisons using Tukey's correction analysis (P = 0.05). In the cell parameters graphs, statistics indicate differences among the different time points evaluated (there is no difference between columns at the same time point). In the focal adhesions parameters and actin graphs, statistics indicate differences between columns of the same condition. *p < 0.05, **p < 0.01, ***p < 0.001, ****p < 0.0001. (For interpretation of the references to colour in this figure legend, the reader is referred to the web version of this article.) (For interpretation of the references to colour in this figure legend, the reader is referred to the web version of this article.)

includes the basement membrane, mainly composed of laminins, collagens, proteoglycans and fibronectin [8]. Fibronectin plays a critical role in muscle regeneration rising massively after muscle injury and contributing to support proliferation and differentiation of muscle stem cells (satellite cells-SCs) [9–11]. In addition to the expression of fibronectin during muscle regeneration, integrins $\alpha_5\beta_1$ and $\alpha_v\beta_3$ play an essential role in the skeletal muscle stability and possess a regulatory role in muscle repair [6,7], as well as in regulating their gene expression by some ion-channels such as potassium channels [38,39].

Fig. 2 shows relative mRNA expression of fibronectin-binding integrins, $\alpha_5\beta_1$ and $\alpha_v\beta_3$. qPCR analysis revealed that active-NaBC1 significantly induced the gene expression levels of $\alpha_5\beta_1$ and $\alpha_v\beta_3$ integrins after 0.5 h, 1 h and 1.5 h, indicating that active-NaBC1 upregulates integrin expression, as we previously described for other cell lines [20,21], and others have also reported as a regulatory function of other ion-channels [40]. We have also confirmed fibronectin-binding integrins upregulation at protein level after NaBC1 activation and confirmed the presence of NaBC1 transporter in C2C12 cellular system (Fig. S3).

Therefore, our findings demonstrate that active-NaBC1 leads to enhanced C2C12 adhesion, inducing larger spreading area correlated with cytoskeleton actin stress fibers and higher number of focal adhesions together with activation of gene and protein expression of $\alpha_5\beta_1$ and $\alpha_v\beta_3$ integrins.

2.2. *Active NaBC1 co-localizes with fibronectin-binding integrins*

The NaBC1, is essential for borate homeostasis and has already been characterized [17]. We recently reported a 3D molecular model of NaBC1 based on the sequence homology of other bicarbonate transporter-related proteins [20]. In the presence of borate, NaBC1

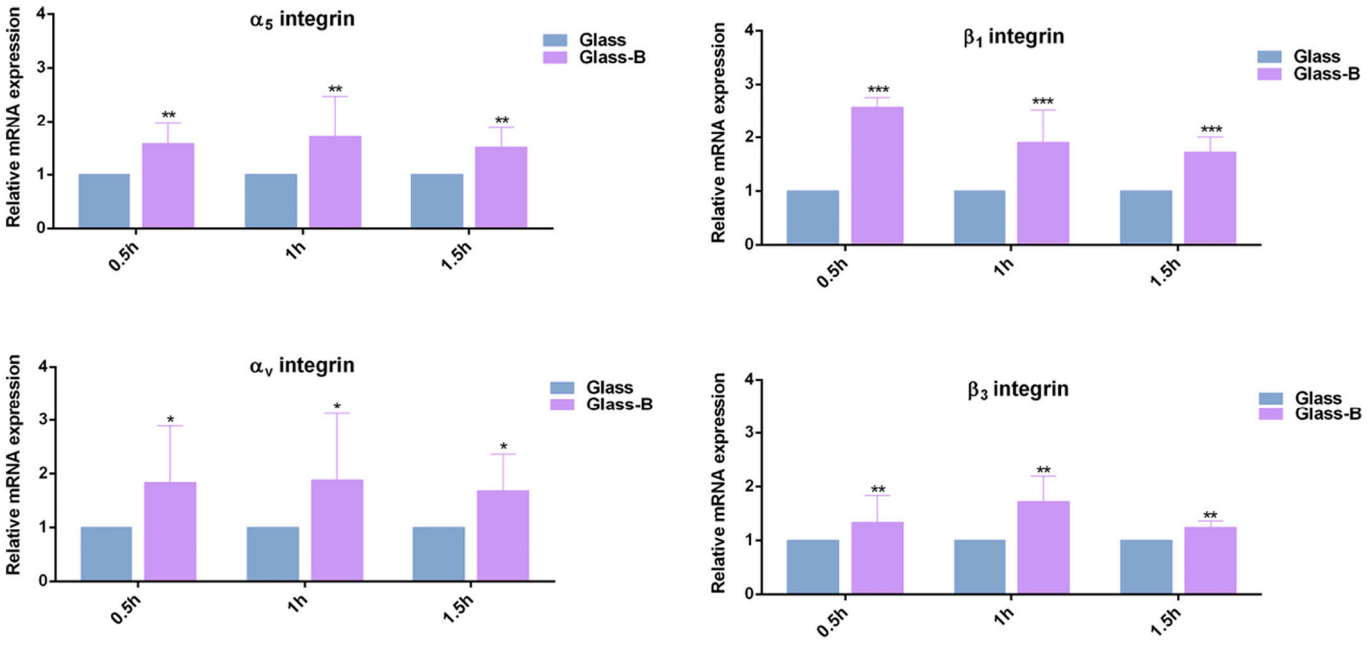

Fig. 2. NaBC1 induces fibronectin-binding integrins expression. C2C12 cells were cultured for 0.5 h, 1 h and 1.5 h onto fibronectin-coated Glass substrates, serum depleted medium and borax (Glass-B) 0.59 mM. qPCR analysis of relative mRNA expression of $\alpha_5\beta_1$ and $\alpha_v\beta_3$ integrins. Active NaBC1 induces fibronectin-binding integrins expression. n = 3 different biological replicas. Statistics are shown as mean ± standard deviation. Data were analyzed by an ordinary two-way ANOVA test and corrected for multiple comparisons using Tukey's correction analysis (P = 0.05). Statistics indicate differences between columns of the same condition. *p < 0.05, **p < 0.01, ***p < 0.001.

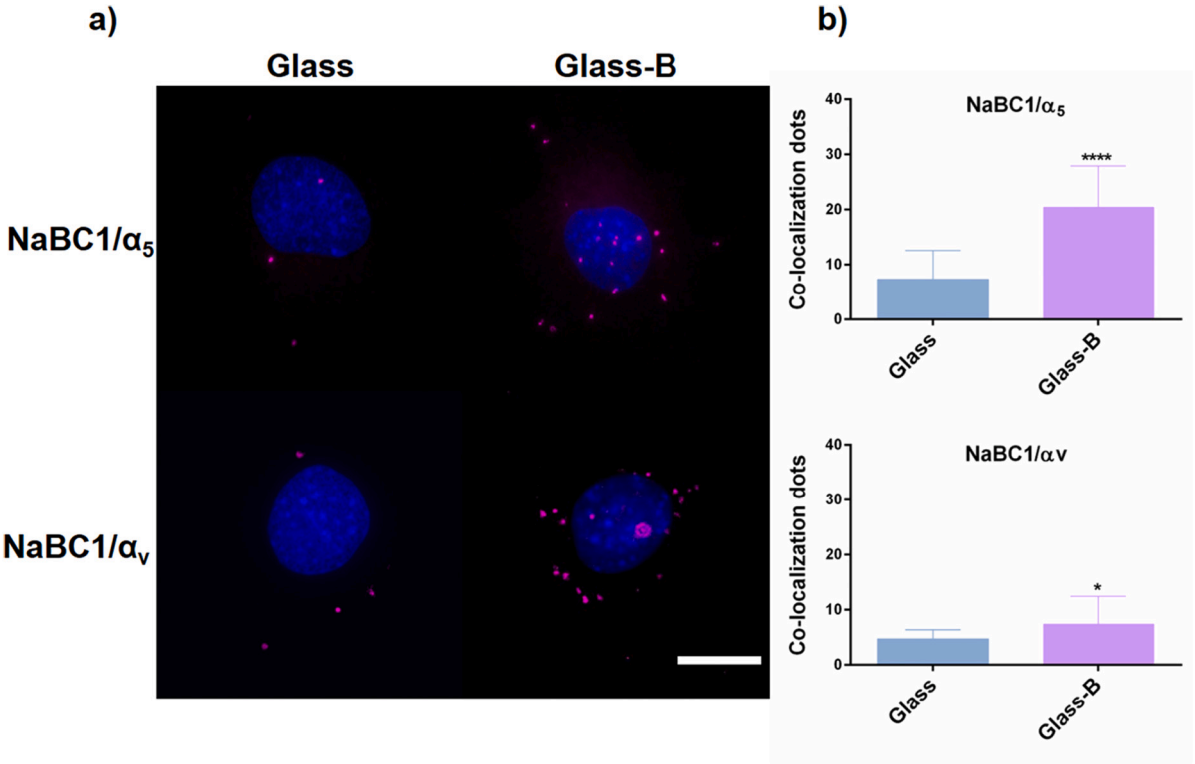

Fig. 3. NaBC1/α_5, α_v integrins co-localization. a) Images of nuclei (blue) and co-localization dots (magenta) of C2C12 cultured for 0.5 h onto fibronectin-coated glass substrates, serum depleted and borax (Glass-B) in the culture medium. Scale bar represents 10 μm. b) Image analysis quantification of the number of co-localization dots of NaBC1/α_5 and NaBC1/α_v. Co-localization levels increased after NaBC1 activation with borax. n = 20 images/condition from 3 different biological replicas. Statistics are shown as mean ± standard deviation. Data were analyzed by an unpaired *t*-test applying Welch's corrections (P = 0.05). *p < 0.05, ****p < 0.0001. (For interpretation of the references to colour in this figure legend, the reader is referred to the web version of this article.)

functions as an obligated Na^+-coupled borate cotransporter. As we used Sodium Tetraborate Decahydrate (borax) dissolved in the medium, we can be confident that borax is the natural ligand for NaBC1 activation disregarding its transport through other mechanisms, such as membrane passive diffusion, as occurs with boric acid [17].

To test whether the simultaneous stimulation of $\alpha_5\beta_1$ and $\alpha_v\beta_3$ integrins and the NaBC1 could follow co-localization, as has previously described for other ion channels [14], we performed NaBC1/α_5–α_v co-localization assays using the DUOLINK® PLA kit system, which shows only the positive signals generated between two different proteins <40 nm apart.

Fig. 3 shows co-localization of NaBC1 with α_5 and α_v integrins after 0.5 h of C2C12 culture. A few fluorescent signal dots appeared in the Glass substrates; however, the positive signals in Glass-B were increased, mainly for α_5 integrin. Considering that fibronectin-binding integrins were already stimulated on all the fibronectin-coated samples, our results indicate that simultaneous stimulation of both receptors promotes an effective co-localization.

Collectively, the results obtained in adherent muscle C2C12 cells demonstrate that borax stimulation of NaBC1 in combination with fibronectin-binding integrins activation potentiate cell adhesion, and further describe a co-localization between NaBC1 and $\alpha_5/\alpha v$ integrins as an adhesion induction mechanism. These findings reinforce our hypothesis suggesting a novel function for NaBC1 besides controlling borate homeostasis.

2.3. Adhesion strength enhanced by active-NaBC1 reduces extracellular fibronectin reorganization and cell migration

Upon an injury, the resident muscle stem cells, called satellite cells

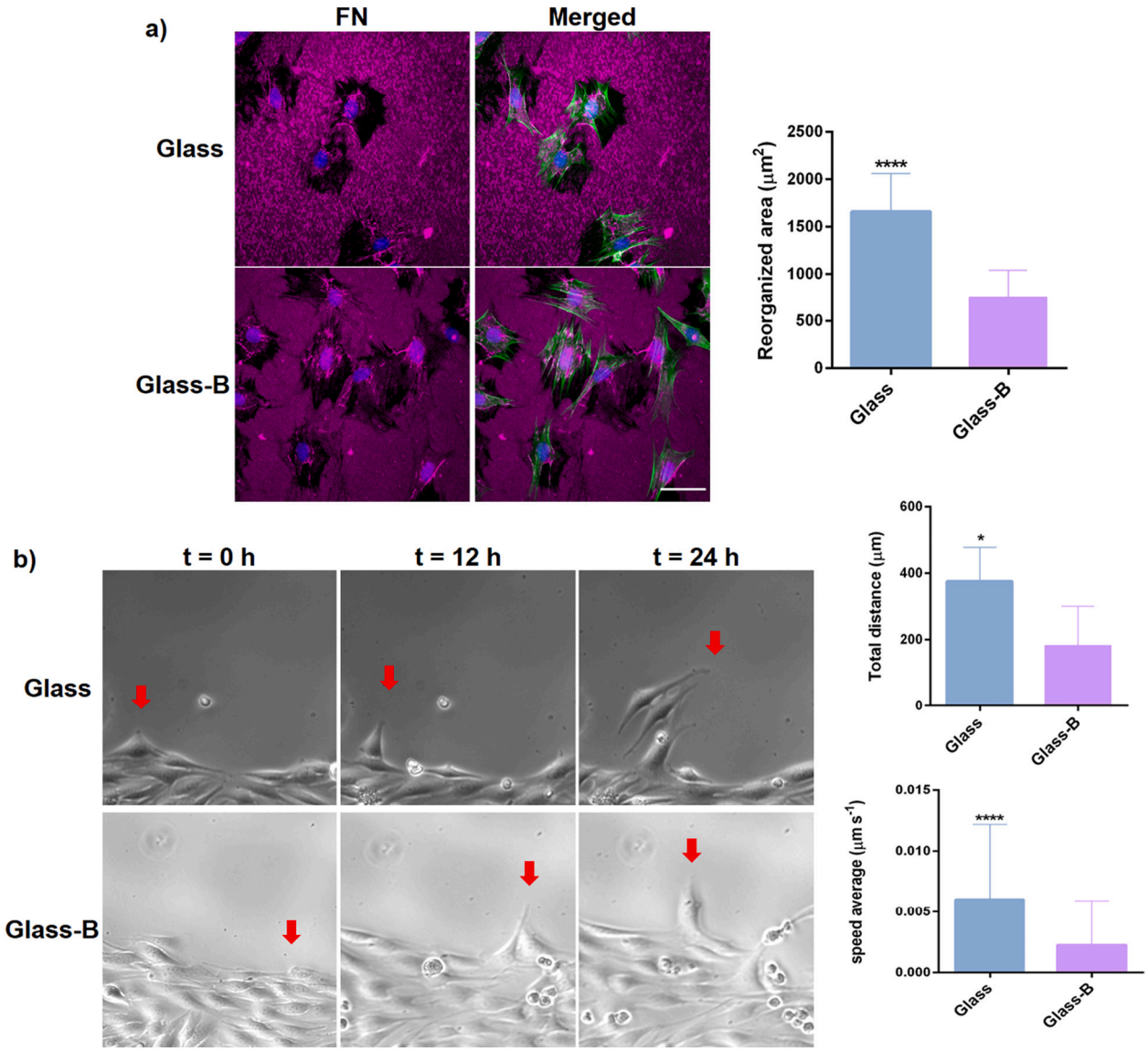

Fig. 4. Characterization of borax effects in extracellular matrix (fibronectin) reorganization and C2C12 cell migration. a) Fibronectin (FN) reorganization by C2C12 cells after 3 h of culture in the presence of serum and borax (Glass-B) in the culture medium. Immunofluorescence detection of fibronectin (magenta), actin cytoskeleton (green) and nuclei counterstained with DAPI (blue). Dark area around each cell was quantified to establish the reorganization area. Scale bar represents 50 µm. n = 10 images from 3 different biological replicas for each condition. b) Phase contrast images of C2C12 representing the position of cells after 0 h, 12 h and 24 h. Red arrows indicate the position of a selected migrating cell over time in the different conditions. Quantification of speed average and total distance covered by tracked cells from time-lapse microscopy experiments (see supplementary videos). n = 6 different tracked cells per condition and 139 measurements per cell for a total of 24 h. Statistics are shown as mean ± standard deviation. Data were analyzed by an unpaired *t*-test applying Welch's corrections (P = 0.05). *p < 0.05, ****p < 0.0001. (For interpretation of the references to colour in this figure legend, the reader is referred to the web version of this article.)

(SCs) start proliferation and differentiate into myoblasts. Myoblasts then proliferate, migrate to the site of injury and differentiate into myotubes that further fuse into preexisting myofibers completing the regeneration process. Since tissue remodeling is a crucial step in muscle regenerative process, we next evaluated whether simultaneous activation of NaBC1 and $\alpha_5\beta_1$ and $\alpha_v\beta_3$ integrins affected ECM reorganization and cell migration. Fig. 4-a shows how C2C12 cells reorganized the pre-adsorbed layer of fibronectin, that appears as a dark area against the fluorescent fibronectin background. Image analysis quantification of the dark areas show reduced levels of fibronectin reorganization after NaBC1 stimulation (Glass-B). Consequently, active-NaBC1 induced a reduced speed average and total migrated distance in time-lapse studies (Fig. 4-b, Supplementary videos). In many cell types, the connection between the adhesion and contraction machineries is essential for an efficient cell migration, and it is widely accepted that larger focal adhesion clusters are typically related to slow moving cells. Our results are in line with these observations indicating that active-NaBC1 enhances the strength of cell adhesion reducing ECM remodeling and speed of cell migration.

2.4. *Active-NaBC1 induces in vitro myotube formation*

Myotube fusion of mononucleated myoblasts is a phase of skeletal myogenesis and is essential for muscle repair. When cultured in low serum conditions, after initial cell adhesion, myoblasts spread, elongate and fuse into multinucleated myotubes. To evaluate the potential of borax to induce myotube formation after NaBC1 activation we detected the expression of sarcomeric α-actinin and quantified the fused myotubes in C2C12 differentiated myoblasts as markers of myogenesis [41]. Fig. 5 shows C2C12 myotubes after 4 days of culture under differentiation conditions (serum-depleted medium and 1% insulin transferrin selenium (ITS)). Despite the initial cell seeding density was equal in both conditions, a factor affecting the level of myogenic differentiation [42], the final total cell number was slightly reduced and the myotube fusion index was significantly higher in the presence of borax (Glass-B) as we previously reported [19].

Sarcomeric α-actinin, among other proteins, contributes with a scaffolding role in integrin-based focal adhesion in muscle tissue [43]. We further evaluated the myotube maturation analyzing myotube ultrastructure with confocal microscopy. Glass-B substrates presented clear sarcomeric α-actinin aligned striations, which were more punctuate in Glass (see Fig. 5 magnification images, central columns). Since myotube maturation is normally associated with the appearance of aligned and structured striations, our results suggest that active-NaBC1 accelerates myotube fusion and maturation.

2.5. *Engineering and characterization of alginate-based hydrogels for borax-release*

With the previous results in mind, we aimed to engineer and characterize alginate-based hydrogels for borax-release. We have already described and characterized a tunable alginate hydrogel material system containing different Na_2HPO_4 salt concentrations in the hydrogel compositions as a gelation retardant. Phosphate salts act as retarding agents due to the ability of phosphate groups to interact with the Ca^{2+} source producing calcium phosphate. This prevents Ca^{2+} ions from reacting with sodium alginate to form the alginate hydrogel and allowed us to obtain an injectable hydrogel to be used in *in vivo* experimentation [44]. We first determined how borax content within alginate hydrogels affected the material properties. Actually, borax chelates Ca^{2+}, expecting in the presence of borax altered gelation times and/or altered borax-release as well as variations in hydrogel mechanical properties. Fig. S4-a, b and c shows the non-cumulative borax-release of 12 mm diameter of non-injectable alginate hydrogels (1.5% alginate) and injectable hydrogels with different Na_2HPO_4 concentrations (0.3 M and 0.5 M).

In order to simulate the *in vitro* conditions used, we loaded the hydrogels by a simple mixing procedure that can be easily translated to

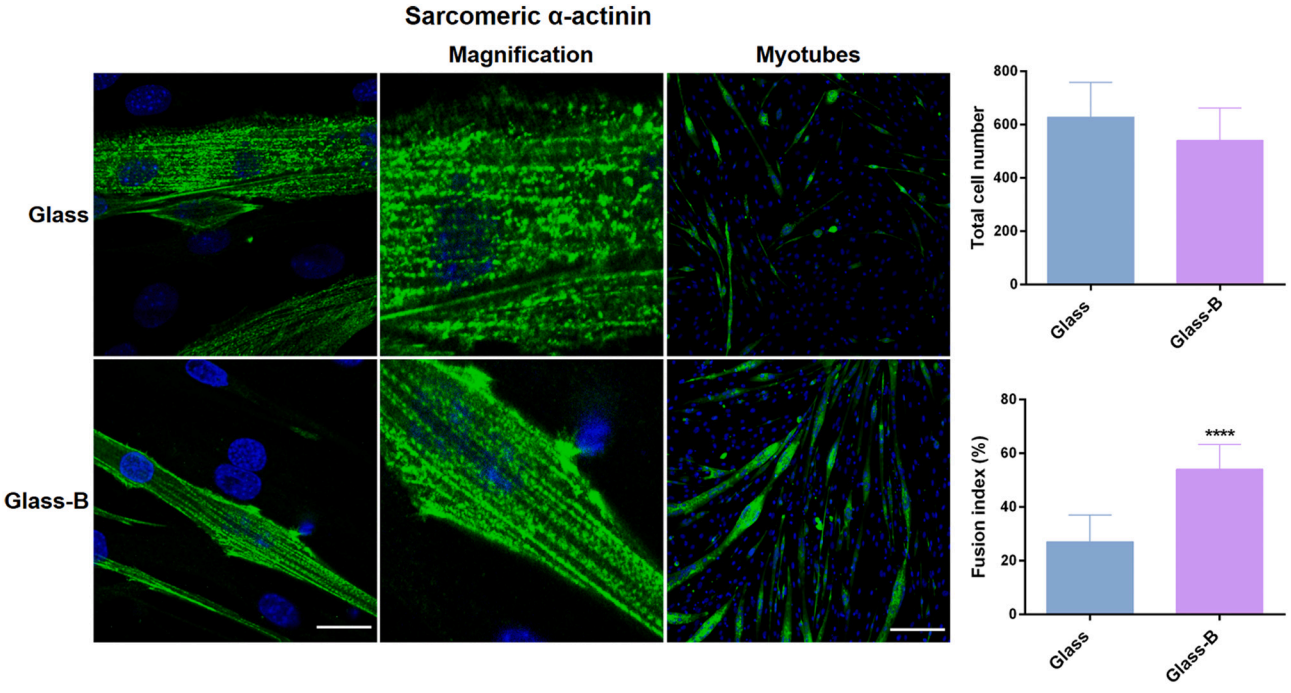

Fig. 5. *In vitro* evaluation of borax effects in C2C12 differentiation. Immunofluorescence images for evaluation of myotube formation using sarcomeric α-actinin as specific muscle marker (green), and counterstained with DAPI (blue) for nuclei visualization. Image analysis quantification of total cell number and the percentage of myotube fusion index. Note that myotubes were defined and counted as cells with three or more aligned nuclei. Active-NaBC1 induces myotube differentiation and sarcomeric aligned striations indicative of myotube maturation. Scale bar for confocal images (left column) 20 μm and for myotubes (right column) 200 μm. n = 10 images from 3 different biological replicas per condition. Statistics are shown as mean ± standard deviation. Data were analyzed by an unpaired *t*-test applying Welch's corrections (P = 0.05). ****p < 0.0001. (For interpretation of the references to colour in this figure legend, the reader is referred to the web version of this article.)

the clinic, with borax 0.59 mM (ALG-B 0.59) and another concentration of 1.47 mM (ALG-B 1.47) to choose the optimal amount to be finally loaded in *in vivo* experiments. Release from ALG-B 0.59 mM and ALG-B 1.47 mM hydrogels resulted in 200 mg L^{-1} and 400 mg L^{-1} at day 1 (Fig. S4-a, b and c), equivalent to 0.52 mM and 1.05 mM respectively, indicating that part of the borax content remains entrapped within the hydrogel and becomes sustained released overtime. The different Na_2HPO_4 concentrations resulted in similar hydrogel behaviors in terms of borax-release, presenting Na_2HPO_4 0.3 M the best injectability properties with a gelation time of 12 min (Supplementary Table 1). Thus, we selected this composition for *in vivo* experiments. We next augmented the borax concentrations for loading the hydrogels to obtain a higher release, considering the partial borax retention observed within the hydrogels and that the size of the implant injected in mice would be reduced to 5 mm instead of 12 mm diameter, meaning that a small hydrogel volume would need more borax-loaded to release the equivalent amount obtained from a big hydrogel volume. Fig. 6-a shows the non-cumulative borax-release from two different loaded compositions of 5 mm injectable hydrogels, concentrations equivalent to ALG-B 0.59 mM and ALG-B 1.47 mM for a reduced implant diameter. Both compositions resulted in an equivalent borax-release of 700 mg L^{-1} (1.8 mM) at day 1, despite their initial loading was performed with two different borax amounts, indicating that ALG-B 1.47 mM solution was saturated and that the maximum amount of borax to be loaded corresponded to 0.59 mM. Although both borax compositions released a similar amount of borax overtime, ALG-B 1.47 mM presented slower release from 2 to 15 days, suggesting that part of the borax content remained within the hydrogel. Additionally we performed a hydrogel-swelling assay showing that the presence of borax within the hydrogel increases water absorption, and that both ALG and ALG-B compositions reach the swelling equilibrium after 24 h (Fig. S4-d). Further, the structural integrity of both hydrogel compositions remained unaltered for >15 days, thus ensuring an optimal implant lifetime for the *in vivo* experiments (Fig. S4-e).

We further evaluated the mechanical properties of the injectable hydrogels (ALG, ALG-B 0.59 mM and ALG-1.47 mM) by rheometry. The complex modulus magnitude ($|G^*| = (G')^2 + (G'')^2$, connected with the stiffness of the material) is independent of deformation for up to 6% strain in all the materials (Fig. 6-b). Accordingly, we chose a strain of 1% for the following experiments to ensure linear viscoelastic behavior [45]. Fig. 6-b shows the evolution of the shear storage and loss moduli as a function of the frequency for the three compositions. Both show an increase with the frequency. We calculated the average values for a fixed frequency in the plateau region, tabulated in Table 1. The data indicate that inclusion of borax within the hydrogels may produce calcium borate particles uniformly dispersed within the hydrogel acting as reinforcement (Fig. 6-b and c), evidenced by the higher values of $|G^*|$ and G' observed in the borax containing hydrogels. In the case of pure alginate, G'' values are lower than in the case of the borax containing

Table 1
Shear storage (G') and loss (G'') moduli at 0.1 Hz and 1% strain for the alginate control without Na_2HPO_4 (ALG), and the Alg-B 0.59 mM and 1.47 mM injectable hydrogels with Na_2HPO_4 0.3 M.

Sample	G' [Pa]	G'' [Pa]
ALG	168 ± 62 (*)	16 ± 5 (*)
ALG-B 0.59 mM	894 ± 321	66 ± 18
ALG-B 1.47 mM	680 ± 115	60 ± 18

Statistics are shown as mean ± standard deviation. Data were analyzed by an ordinary one-way ANOVA test and corrected for multiple comparisons using Tukey's correction analysis (P = 0.05). *p < 0.05.

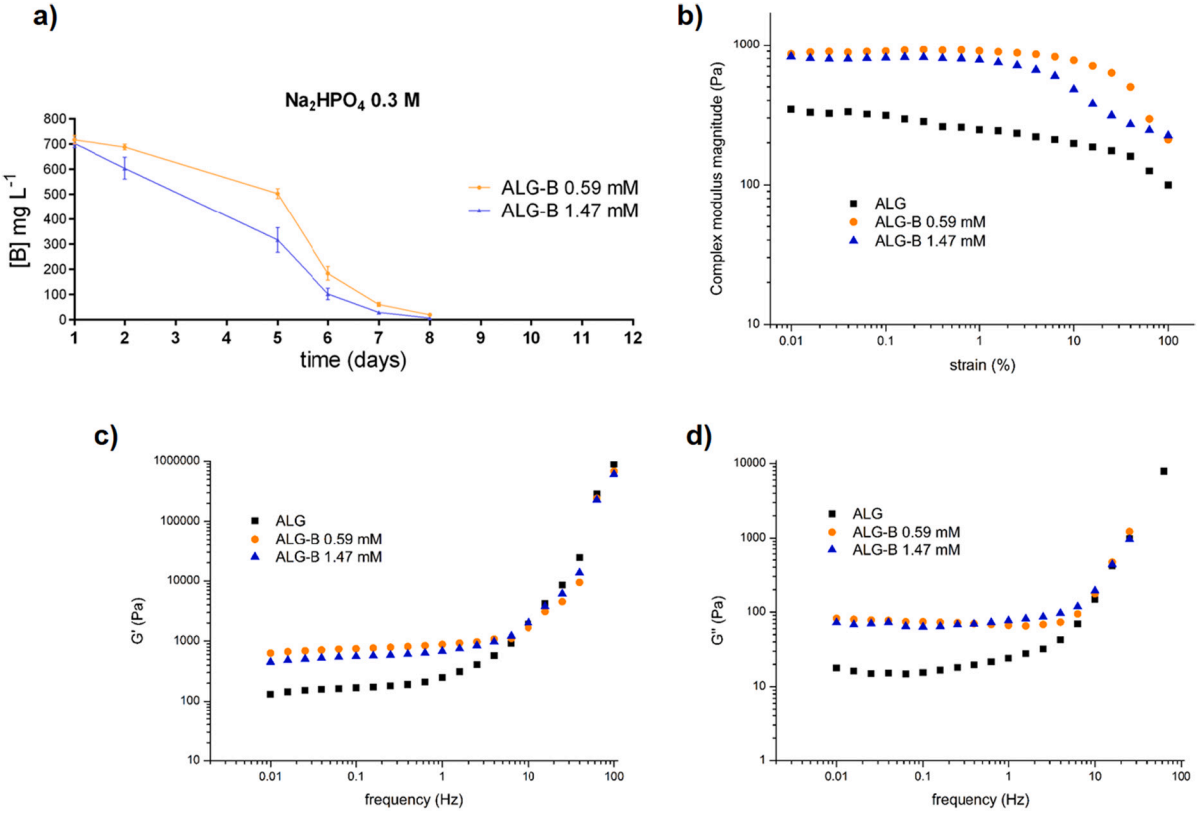

Fig. 6. Characterization of hydrogel material systems for *in vivo* experimentation. a) Long-time non-cumulative borax-release assay of 5 mm injectable ALG-B 0.59 mM and 1.47 mM hydrogels after 1, 2, 5, 6, 7 and 8 days. b) Dependence of the complex modulus magnitude ($|G^*|$) on the strain amplitude at 1 Hz. c) Evolution of the shear storage (G') and d) loss (G'') moduli as a function of the frequency at 1% strain amplitude for the Alg-B 0.59 mM and 1.47 mM injectable hydrogels with Na_2HPO_4 0.3 M and alginate control without Na_2HPO_4. Each curve corresponds to the average of three different replicates.

hydrogels probably due to the dissipation provided by the formed salts. No differences in the modulus is observed between ALG-B 0.59 mM and ALG-B 1.47 mM hydrogels, confirming that solution of ALG-B 1.47 mM is saturated and both hydrogel compositions contain similar amount of borax.

2.6. Active-NaBC1 enhances muscle regeneration after an injury in vivo

Taking into account the rheometry results indicating that both ALG-B 0.59 and 1.47 mM hydrogel compositions have similar behavior in terms of mechanical properties, and the release results showing that both compositions contain and release similar amount of borax, we thus selected just ALG-B 0.59 mM, named as ALG-B herein after for *in vivo* experiments. Additionally, we also tested ALG-B hydrogels cytotoxicity in direct contact with cells to ensure the viability of the material systems in the C2C12 muscle cell line in differentiation conditions. Fig. S5 shows C2C12 viability in direct contact with ALG and ALG-B hydrogels, indicating that neither ALG nor borax released from ALG-B hydrogels are cytotoxic.

Given our original *in vitro* results obtained in C2C12 cells, we next wonder how active-NaBC1 would participate in muscle regeneration process in an *in vivo* mouse model of muscle regeneration after inducing an acute injury with cardiotoxin (CTX). CTX is a snake myotoxin, which after intramuscular injection induces myolysis of myofibers triggering a local response and reproducing muscle regeneration events [46].

Skeletal muscle damage was induced by CTX injection in the tibialis anterior muscle of mice [47]. We evaluated three different groups (6 mice/group) composed by control wild type mice, CTX injured mice with alginate implant (ALG) and CTX injured mice with alginate-borax implant (ALG-B). After 3 days of injury, hydrogel material systems were subcutaneously injected in the same location of injury. Fig. 7 shows representative histological and immunohistochemical images of tibialis anterior muscle sections isolated after 15 days of regeneration process. It is important to note, that at this time point, the structural architecture of the muscle is completely repaired and no inflammation signals can be detected [47]. We evaluated the eosinophilic regenerating myofibers characterized by centrally located nuclei in distinction of the complete regenerated myofibers categorized by peripheral located nuclei under the sarcolemma (wild type Control). Although both ALG and ALG-B implants resulted in augmented regenerating myofibers compared with the uninjured group (Control) due to the provoked CTX injury, the presence of borax within the implant resulted in a significant increase of the total nuclei, centrally located nuclei (indicative of *de novo* formation of multinucleate myofibers) and cross-sectional area (CSA) of regenerating fibers. Indeed, analysis of CSA distribution indicates that ALG-B presented the major number of fibers with an increased CSA, associated with an improved and accelerated regenerative response. It is important to highlight that the CSA trend observed in ALG-B implants after 15 days of injury is similar to the trend obtained in the time course analysis of reported skeletal muscle regeneration studies after 30 days of injury [47], reinforcing our affirmation that active-NaBC1 is improving and accelerating muscle regeneration events.

To further confirm the histological observations we evaluated tibialis anterior sections by immunofluorescence for muscle markers related to muscle repair processes. Chloride-channel-1 (CLC-1) predominantly expressed in skeletal muscles whose genetic defects cause myotonia and several rare muscle diseases (Becker's disease, Thomsen's disease); [48] Laminin, a major component of muscle basal lamina and CD31 a vascular marker essential in muscle regenerative processes. Both, laminin and CD31, become disrupted after an injury and reconstitute progressively during muscle repair [46].

The presence of borax within the implant resulted in a significant increase in the CLC-1, laminin and CD31 markers (Fig. 7-b). CLC-1 and laminin levels in ALG implant were similar to uninjured control, indicating that ALG alone had no effects on muscle regeneration. CD31 strongly decreased (ALG) and fibronectin increased (ALG and ALG-B) after CTX injury as expected, compared to uninjured control. Interestingly, the levels obtained in the CLC-1, laminin and CD31 markers in ALG-B implants resulted in a significant increase compared to both ALG and healthy control. In particular, the elevated levels of laminin and CD31 markers after CTX injury, and comparing to bare ALG, suggest that the presence of borax is accelerating the progressive reconstitution that takes place during muscle repair. Altogether, our findings in mice demonstrates that borax-loaded injectable alginate implants are capable of effective stimulation of NaBC1 *in vivo* producing an effective muscle regeneration process and accelerating muscle repair.

3. Discussion

Muscle tissue engineering seeks to develop tissue-like scaffolds to enhance new muscle formation from remaining tissue *in vivo*. Understanding the role of muscle ECM and its interactions with cellular membrane receptors is critical for the success of the current approaches aiming to mimic more precisely the native muscle niche. Diverse strategies have been used for muscle tissue engineering comprising scaffold-based strategies (composed of natural [49–53] and synthetic polymers [54–56]), cell-based [57–61] strategies, molecular signaling-based strategies mainly focused in growth factor delivery [62–67] or a combination of cells and growth factors [68] to drive endogenous skeletal muscle regeneration. However, scarce reports describe material systems for ion-delivery to stimulate intracellular signaling [32–35] and no available information exist regarding hydrogel-based material systems for borax delivery as a bioactive molecule for skeletal muscle repair. Despite significant progress have been made towards the understanding of the molecular mechanisms of muscle regeneration in damaged muscles or muscle diseases, all the current therapies present important shortcomings without clear success.

As has been broadly described in the literature, ion channels and ion transporters are key transmembrane proteins participating in muscle physiology. Intracellular and extracellular Ca^{2+}, K^{+}, Na^{+} and Cl^{-} ions distribution play a pivotal role in cell migration, myotube fusion and muscle contraction/relaxation [15,16,69,70]. Ion channel function impairment in skeletal muscle may lead to muscular and neuromuscular diseases [71,72].

Even though the reports describing the importance of the most abundant ions in organisms participating in physiological and signaling processes, whether other ion transporters highly specialized in the transport of trace elements such as borates participate in intracellular signaling, besides controlling cell homeostasis, is still not clear. Some reports describe the essentiality of boron as a nutrient in mammalian organisms [73]. The borate transporter, NaBC1, described as a tight coupled $Na^{+}/B(OH)_4^{-}$ co-transporter, has been defined as an ideal boron-concentrating pump, reinforcing the idea of the essentiality of this trace element for mammalian cells [17]. Mutations in NaBC1 cause genetic rare diseases in humans [18,19]. However, the role of NaBC1 participating as more than a merely borate transporter is unknown to date. Only recently, we have predicted a 3D-protein structural model for NaBC1 transmembrane protein, and described a novel function for this transporter, participating in combination with fibronectin-binding integrins and growth factor receptors enhancing vascularization *in vitro* and *in vivo* [20] and inducing an adhesion-driven state in Mesenchymal Stem Cells generating intracellular tension inducing osteogenesis [21]. In the present study, we present a simple approach that promotes muscle regeneration *in vitro* and *in vivo*. We demonstrate *in vitro* that the simultaneous activation of NaBC1 and fibronectin-binding integrins, induces an adhesion-driven state of C2C12 cells, enhancing cell adhesion in terms of greater cell spreading and the formation of focal adhesions (number and area) (Fig. 1), generating longer and mature focal adhesions at the early stages, as well as higher expression of actin stress fibers leading to nuclear deformation, suggesting nuclear stress and activation of intracellular tension (Fig. S2). Previous evidence pointed to the orchestrated crosstalk between actin cytoskeleton and its

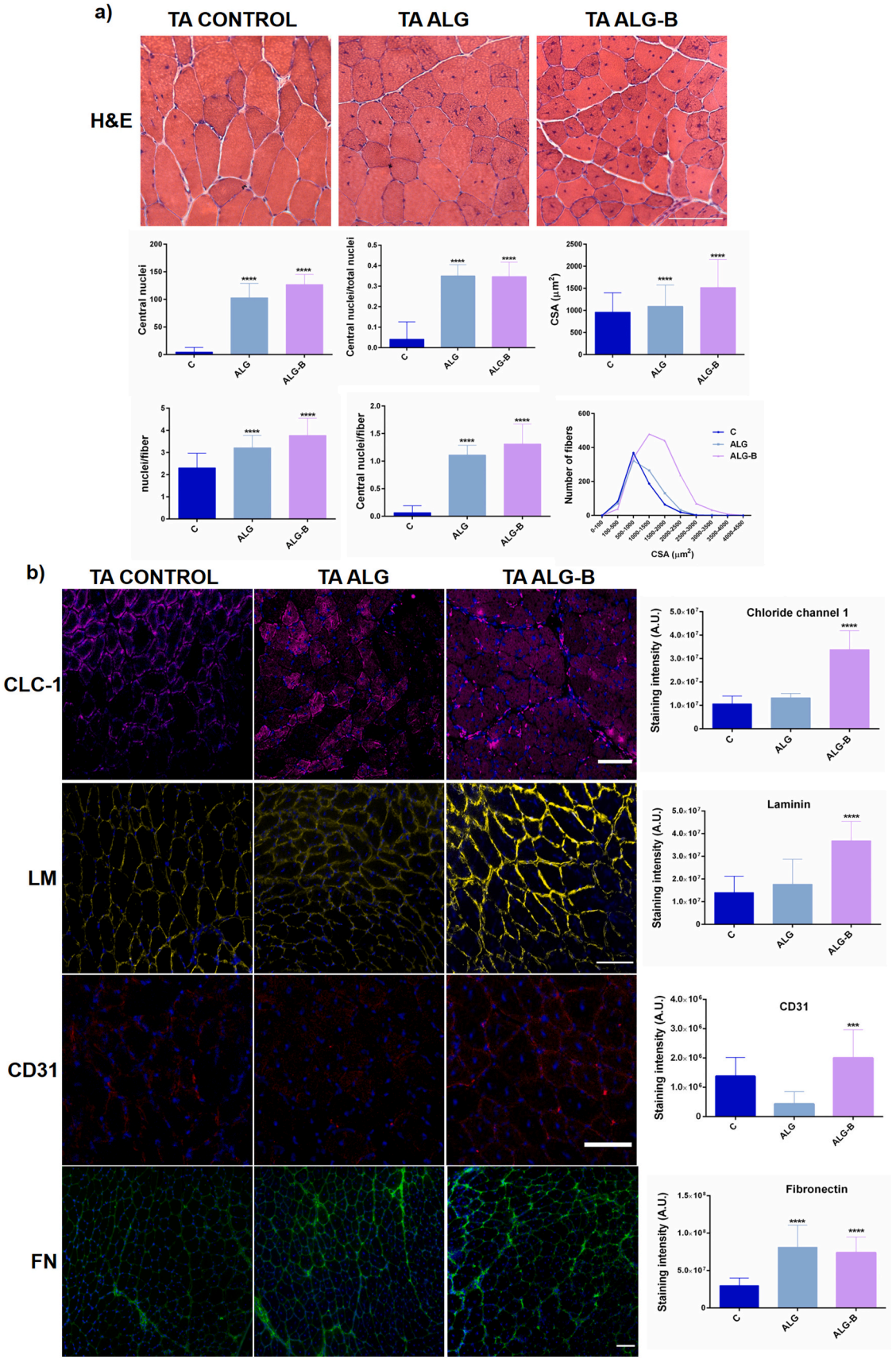

(caption on next page)

Fig. 7. Evaluation of the borax effects in skeletal muscle regeneration in a mouse model of acute injury with cardiotoxin (CTX). a) Analysis of tibialis anterior (TA) muscle regeneration 15 days after injury by Hematoxylin & Eosin staining. Images show representative regenerating myofibers with centrally located nuclei (ALG and ALG-B). Tibialis anterior control represents healthy tissue without induced muscle injury. Note the myofibers with periphery located nuclei. Scale bar 200 μm. Image analysis quantification of regenerating myofibers in the different conditions. Active-NaBC1 significantly increases regenerating fibers characterized by the presence of centrally located nuclei. n > 70 images from 6 different mice per condition. Image analysis quantification for morphological evaluation of the regenerating myofibers. Active-NaBC1 significantly increases myofiber cross-sectional area (CSA) associated with an accelerated regenerative response. n > 700 fibers from 6 different mice per condition. Statistics are shown as mean ± standard deviation. Data were analyzed by an ordinary one-way ANOVA test and corrected for multiple comparisons using Tukey's correction analysis (P = 0.05). Statistics indicate differences between groups. ****p < 0.0001. b) Immunohistochemically stained tibialis anterior sections for evaluation of different markers related to muscle regeneration using Chloride channel (CLC-1 - magenta), laminin (LM - yellow), CD31 (red) and fibronectin that raises after an injury (FN – green) counterstained with DAPI (blue) for nuclei visualization. Image analysis quantification of the integrated density as a measure of the total detected fluorescence. Active-NaBC1 promotes higher expression of CLC-1, laminin and CD31 indicative of an accelerated regenerative response. Scale bar 100 μm. n = 10 images from 3 different mice per condition. Statistics are shown as mean ± standard deviation. Data were analyzed by an ordinary one-way ANOVA test and corrected for multiple comparisons using Tukey's correction analysis (P = 0.05). ****p < 0.0001. (For interpretation of the references to colour in this figure legend, the reader is referred to the web version of this article.)

many regulators for a successful myoblast fusion, describing that accumulation of polymerized actin and vinculin is essential for myotube formation [74]. These described evidences are in line with our results, showing that the enhanced adhesion state generated after simultaneous activation of NaBC1 and fibronectin-binding integrins leads to improvement of myotube fusion and maturation after C2C12 differentiation (Fig. 5).

Previous data also report a contributing role for integrin family members in myoblast adhesion, alignment and fusion [6,7], highlighting the role of β_1 integrin in the fusion of myoblasts with nascent myotubes [74]. We have demonstrated that the presence of borax induces the expression of $\alpha_5\beta_1$ and $\alpha_v\beta_3$ integrins at mRNA and protein levels (Figs. 2 and S3). Furthermore, the simultaneous stimulation of both membrane receptors (NaBC1/$\alpha_5\beta_1$/$\alpha_v\beta_3$) followed their co-localization (Fig. 3), as we have previously reported in other cellular systems [20,21] and has been described for other ion channels [14], strongly suggesting a cooperation mechanism between them.

ECM reorganization and cell migration are linked events essential for muscle repair. Connection between the integrin-mediated adhesion and contraction proteins involved is necessary for an efficient cell movement. Moreover, it is reported that some ion channels (*i.e.* K^+ channels) can regulate cell migration by forming molecular complexes with integrins [75]. We obtained reduced levels of fibronectin reorganization and speed average as well as total migrated distance in time-lapse studies (Fig. 4) after simultaneous activation of NaBC1/fibronectin-binding integrins. It is broadly accepted in the literature a direct relation between focal adhesion size and migration, meaning that large focal adhesion clusters are typical of slow moving cells [16]. Our results are in agreement with those findings describing the importance of focal adhesion size in cell movement and in generation of tractional forces by cells [76]. The adhesion-driven mechanism induced by active NaBC1, increasing the number of mature focal adhesions, the spreading area and actin cytoskeleton at early initial steps corroborates that focal adhesion size does matter as previously reported [77], and strongly supports the hypothesis that active NaBC1 induces a more robust strengthening response of the cells. Therefore, despite slow migration rates and less reorganized fibronectin compared to control, still, cells are able to reorganize and migrate indicating that these essential properties are not altered for the accomplishment of their biological functions in muscle regeneration.

We further demonstrated that active NaBC1 induces an improved and accelerated muscle repair *in vivo*. We selected cardiotoxin (CTX) as an injury model among others such as freeze injury, $BaCl_2$ or notexin, because avoids a persistent inflammation and allows the reproducibility of the synchronous process of muscle regeneration [46]. We have engineered an injectable alginate-based hydrogel material system, novel in the function for borax delivery, by a simple mixing procedure to drive endogenous skeletal muscle regeneration. Material characterization demonstrates that borax-loaded hydrogels maintained a sustained borax-release overtime and achieved high mechanical strength while still keeping their injectability and biocompatibility properties (Fig. 6). After CTX injury, the alteration of tissue and blood vessels produce inflammation and generates a hematoma that contains large amounts of plasma-derived fibronectin, which provides a scaffold for new ECM formation and an anchorage site for infiltrating inflammatory cells and other multiple growth factors and molecules implicated in muscle regeneration [9]. Thus, we have ensured and demonstrated fibronectin presence in our material system for simultaneous stimulation of fibronectin-binding integrins and borax for NaBC1 stimulation after CTX injury (Fig. 7-b). Results from *in vivo* experimentation show that the presence of borax within the hydrogel strongly induced muscle repair, by means of increased number of *de novo* formed myofibers (with centrally located nuclei) and cross-sectional area (CSA) (Fig. 7-a). Increased myofibers CSA is associated with an improved and accelerated regenerative response while a decreased CSA is indicative of a failure of proper regeneration. CSA shifts towards larger-sized fibers as the process of regeneration proceeds with time, demonstrating that the results obtained with ALG-B implant (15 days post-injury, Fig. 7-a) are accelerating the regenerative process presenting a trend similar to that obtained after 30 days of injury [47]. To verify these findings we explored the analysis of muscle markers related to muscle repair. The results show that NaBC1 activation by ALG-B implant induced elevated levels of CLC-1, laminin and CD31 (Fig. 7-b), specifying NaBC1 activation in the promotion of muscle regeneration. The remodeling of connective tissue and angiogenesis defines an advanced stage of the regenerative process (occurring after 15 days of injury), characterized by the overproduction of several types of ECM proteins such as laminin and new vascular network [2]. Thus, the observation of elevated levels after CTX injury of CLC-1, laminin and CD31 was expected after implantation of both ALG and ALG-B implants. However, the fact that those markers were highly overexpressed only after ALG-B implants strongly suggest that active NaBC1 accelerates the normal stages of reconstitution of injured muscle.

We have therefore demonstrated a novel function for the NaBC1 transporter in muscle tissue. Here we propose a simple approach, easily translatable to the clinic, for driving muscle regeneration through a mechanism that involves the simultaneous stimulation of NaBC1 and fibronectin-binding integrins to enhance intracellular signaling. Our results indicate an adhesion-driven state, resulting in enhanced myotube formation, and involved a crosstalk mechanism between cellular membrane receptors. To date, the synergistic interactions between ion channels/transporters and integrins have not been exploited to engineer material systems for biomedical applications. Our findings open up new ways for engineering biomaterials to be employed in biomedical applications for muscle repair after muscle injury, muscular dystrophies or muscle aging.

4. Conclusions

This work proposes a novel way to potentiate muscle regeneration using the interplay between specific cell membrane receptors. Our data demonstrate that the simultaneous stimulation of NaBC1 and fibronectin-binding integrins generates an adhesion-driven state,

inducing focal adhesion formation, cell spreading and focal adhesion size leading to nuclear deformation suggesting intracellular tension at early adhesion stages, strengthening myoblast attachment as a determinant affecting myotube fusion and maturation. This stimulation further accelerates the muscle repair processes *in vivo*. We describe a novel mechanism involving the crosstalk and co-localization of active NaBC1/$\alpha_5\beta_1$/$\alpha_v\beta_3$ integrins, with a novel function for NaBC1 transporter in muscle regeneration, besides controlling boron homeostasis.

5. Experimental section

5.1. Material substrates

Cleaned glass cover slips were used as 2D substrates for *in vitro* experiments. Sodium Tetraborate Decahydrate Borax 10 Mol (hereafter borax - B -) ($Na_2B_4O_7{\cdot}10H_2O$, Borax España S.A) was dissolved in the culture medium in all the *in vitro* experiments at concentration of 0.59 mM. Ultrapure sodium alginate with molecular weight of 75–200 kDa and Guluronate/Mannuronate ratio $\geq$ 1.5 were purchased from FMC Biopolymer. Calcium sulphate dihydrate ($CaSO_4{\cdot}2H_2O$), was purchased from Sigma-Aldrich. Di-sodium hydrogen phosphate dihydrate ($Na_2HPO_4{\cdot}2H_2O$) was purchased from Panreac.

All the 2D substrates were functionalized with human plasma fibronectin (Sigma-Aldrich). After sterilizing with UV for 30 min, the substrates were coated with 20 μg mL^{-1} fibronectin solution in Dulbecco's Phosphate Saline Buffer (DPBS) for 1 h at room temperature.

5.1.1. Alginate-based hydrogel preparation

Ultrapure sodium alginate (FMC Biopolymer), was dissolved in 1% (*w/v*) D-mannitol aqueous solution (Sigma-Aldrich) at a concentration of 1.5% (w/v). Borax was dissolved in different alginate solutions at 0.59 mM or 1.47 mM concentrations. All alginate solutions were next filtered through a 0.22 μm pore Minisart Syringe Filter (Sarto-rius). For gelation, 2.7 mL of the alginate solutions were mixed with 60 μL of 1.22 M $CaSO_4{\cdot}2H_2O$ (Sigma-Aldrich) through two Luer Lock syringe (BS Syringe) connected with a Fluid Dispensing Connector (Braun). Alginate and $CaSO_4{\cdot}2H_2O$ were mixed 15 times until complete homogenization. To retard the gelation time, 60 μL of either 0.3 M or 0.5 M $Na_2HPO_4{\cdot}2H_2O$ (Panreac) were added in the cross-linking reaction.

5.2. Material characterization

5.2.1. Rheometry

Cylindrical hydrogels were prepared by crosslinking the alginate in 8 mm diameter agarose molds. After crosslinking, they were kept at 4 °C until measured. Rheological experiments were performed on a strain-controlled Discovery HR-2 rheometer (TA Instruments) at 4 °C. Samples were placed between two parallel plates of nonporous stainless steel. The gap between the plates was adjusted using a normal force of 0.1 N to prevent slippage. Temperature was controlled by a Peltier device situated in the lower plate.

Two types of measurements were made in the in shear deformation mode. First, the range of strain amplitudes for which hydrogels exhibit linear viscoelastic behavior was determined. A dynamic strain sweep, with amplitudes ranging between 0.01% and 100%, at the frequency of 1 Hz was implemented. The dynamic shear modulus as a function of the strain was recorded. Second, a dynamic frequency sweep was applied to determine the dependence of the shear storage modulus (G′) and loss modulus (G″) on frequency. The frequency varied from 0.01 Hz and 100 Hz at the selected strain of 1% in the linear region. Three replicates per sample were measured.

5.2.2. Water absorption

Hydrogels were formed, weighed (m0) deposited in a p-24 multiwell plate and immersed in 1 mL of ultra-pure miliQ water for 72 h. Samples were weighed after removing the liquid supernatant at different time points of 2 h, 24 h 48 h and 72 h. The amount of water adsorbed was calculated as follows:

$$Water\ Sorption\ (\%) = \frac{mt–m0}{m0} \times 100$$

where mt is the weight of the hydrogel at the different time points and m0 the weight of the hydrogel after gelation. Three replicates per sample were measured.

5.2.3. Borax-release determination

The *in vitro* release of borax was performed immersing the different alginate-based hydrogels (Alg, Alg-B 0.59 mM and Alg-B 1.47 mM), prepared with the different compositions in terms of Na_2HPO_4 content (0.3 and 0.5 M), in 1 mL of ultra-pure water, DPBS without Ca^{2+} and Mg^{2+}, and DPBS with Ca^{2+} and Mg^{2+} (Gibco). All hydrogels were mixed as described above and performed with identical mass and diameter using agarose 2% (w/v) molds. Hydrogels of 12 mm diameter were used for the determination of the best B concentrations for loading alginate gels, and hydrogels of 5 mm were used for *in vivo* experiments. Long-term release studies (maximum time 19 days) were performed simulating a 19 days cell culture in humidified atmosphere at 37 °C and 5% CO_2. Aliquots consisting of the total amount of immersing liquid (1 mL) were removed from the plates after diverse time points. Reaction of the borax present in the collected aliquots with azometin (Sigma) in acid medium (KAc/HAc buffer pH 5.2) originates a colorimetric reaction measured at 405 nm in a Victor III (Perkin Elmer) device. Standards for calibration were prepared at concentrations of 0, 0.1, 0.25, 0.5, 1, 1.5, 2.5, 5, 10, 25, 50 and 500 mg mL^{-1} of B, using 40 μL aliquots from the original standard solutions for colorimetric reactions. Three replicates per sample were measured.

5.3. In vitro C2C12 muscle cell culture

Murine C2C12 cells (Sigma-Aldrich) were maintained in Dulbecco's Modified Eagle Medium (DMEM, Invitrogen) with high glucose content, supplemented with 20% Fetal Bovine Serum (FBS, Invitrogen) and 1% antibiotics (P/S) (1 mL of a mixture of 10,000 units mL^{-1} of penicillin and 10,000 μg mL^{-1} streptomycin per 100 mL of media, Thermofisher) in humidified atmosphere at 37 °C and 5% CO_2. Cells were sub-cultured before reaching confluence (approximately every 2 days).

5.4. Cytotoxicity assay

MTS quantitative assay (The CellTiter 96 Aqueous One Solution Cell Proliferation Assay, Promega) was performed to assess cytocompatibility of borax with C2C12 cells and to establish the maximum working concentrations to use with this particular muscle cell line. 20,000 cells cm^{-2} were seeded onto a p-24 multi-well plate and metabolic activity was measured after 48 h of incubation of cells with different quantities of borax in media (0.2, 0.6, 3, 6, 10 and 20 mg mL^{-1}) in DMEM supplemented with 1% P/S and 2% FBS (low serum concentration for inducing differentiation conditions). Cells were then incubated for 3 h with MTS (tetrazolium salt) at 37 °C and the formation of formazan was followed by measuring absorbance at 490 nm. All measurements were performed in triplicate.

MTS assay was also performed following the same procedure to test cytotoxicity of ALG and ALG-B injectable hydrogels in direct contact with cells for 48 h under differentiation conditions. Three replicates per sample were measured.

5.5. Cell adhesion

For cell adhesion experiments, C2C12 cells were seeded at low density of 5.000 cells cm^{-2} onto fibronectin functionalized glass substrates. Cells were cultured in DMEM with high glucose content, 1%

(penicillin/streptomycin) antibiotics and in absence of serum (FBS). Samples were also supplemented with borax 0.59 mM as required. After 0.5, 1 and 1.5 h of culture, cells were washed in DPBS (Gibco) and fixed in 4% formaldehyde solution (Sigma-Aldrich) for 30 min at 4 °C. Three biological replicas were evaluated.

5.6. Cell differentiation

For differentiation experiments, C2C12 cells were plated on glass fibronectin-coated substrates at high seeding density of 20,000 cells cm^{-2}, directly under differentiation conditions for myotube formation in the absence of serum and DMEM supplemented with 1% Insulin-Transferrin-Selenium (ITS, Gibco) and borax 0.59 mM as required. After 4 days of culture, cells were washed in DPBS (Gibco) and fixed in 4% formaldehyde solution (Sigma-Aldrich) for 30 min at 4 °C. Three biological replicas were evaluated.

5.7. Matrix reorganization and migration studies

C2C12 cells were seeded at 5.000 cells cm^{-2} onto fibronectin-coated glass cover slips and in the presence of 10% FBS to allow cells to reorganize the adsorbed fibronectin. After 3 h of culture, cells were washed with DPBS (Gibco) and fixed in 4% formaldehyde solution (Sigma-Aldrich) for 30 min at 4 °C. Following the same procedure explained in the immunofluorescence assay section, samples were incubated with primary antibody against fibronectin (Sigma-Aldrich, 1:400) and Cy3-conjugated anti-mouse secondary antibody (Jackson Immunoresearch, 1.200) and BODIPY FL phallacidin (invitrogen, 1:100) for visualization of fibronectin and cell cytoskeleton. Nuclei were counterstained with Dapi. Nikon Eclipse 80i fluorescent microscope was used for cellular imaging. Three biological replicas were analyzed.

For migration experiments, C2C12 cells were starved overnight for synchronization (ultra-low serum conditions 1% FBS). 5.000 cells cm^{-2} were seeded onto fibronectin-coated glass cover slips and in the absence of FBS. The plate was disposed in the monitored staged of a Leica DMI6000 time-lapse microscope for recording of cell movements. Images were recorded every 10 min for 24 h. Six migrating cells from two time-lapse videos per condition were analyzed using the imageJ software.

5.8. Immunofluorescence assays

Cells from adhesion, differentiation or reorganization experiments were rinsed with DPBS and permeabilized with DPBS/0.5% Triton x-100 at room temperature for 5 min, next blocked in 2% BSA/DPBS for 1 h at 37 °C, and then incubated with primary antibodies in blocking solution overnight at 4 °C. The samples were then rinsed twice in DPBS/0.1% Triton X-100 and incubated with the secondary antibody and/or BODIPY FL phallacidin (Invitrogen, 1:100) at room temperature for 1 h. Finally, samples were washed twice in DPBS/0.1% Triton X-100 before mounting with Vectashield containing DAPI (Vector Laboratories) and observed under an epifluorescence microscope (Nikon Eclipse 80i).

For cell adhesion studies, monoclonal primary antibody against vinculin for focal adhesion detection (Sigma-Aldrich, 1:400) and Cy^3 conjugated (Jackson Immunoresearch, 1:200) secondary antibodies were used.

For differentiation studies, monoclonal primary antibody against sarcomeric α-actinin (Abcam, 1:200) and anti-mouse Cy3-conjugated secondary antibodies (Jackson Immunoresearch, 1:200) were used.

5.9. Gene expression

Total RNA was extracted from C2C12 cultured for 0.5, 1 or 1.5 h under different experimental conditions using RNeasy Micro Kit (Qiagen). RNA quantity and integrity was measured with a NanoDrop 1000 (ThermoScientific). Then 500 ng of RNA were reverse transcribed using the Superscript III reverse transcriptase (Invitrogen) and oligo dT primer (Invitrogen). Real-time qPCR was performed using Sybr select master mix and 7500 Real Time PCR system from Applied Biosystems. The reactions were run at least in triplicate for both technical and biological replicas. The primers used for amplification were designed from sequences found in the GenBank database and included:

Integrin α_5 (NM_010577.3, Forward: 5′-GGA CGG AGT CAG TGT GCT G-3′, Reverse: 5′-GAA TCC GGG AGC CTT TGC TG-3′), Integrin β_1 (NM_010578, Forward: 5′-CAT CCC AAT TGT AGC AGG CG-3′, Reverse: 5′-CGT GTC CCA CTT GGC ATT CAT-3′), Integrin α_v (NM_008402.2, Forward: 5′-CAC CAG CAG TCA GAG ATG GA-3′, Reverse: 5′-GAA CAA TAG GCC CAA CGT TC-3′), Integrin β_3 (NM_016780.2, Forward: GGA ACG GGA CTT TTG AGT GT-3′, Reverse: 5′-ATG GCA GAC ACA CTG GCC AC-3′). β-actin (NM_007393.3, Forward: 5′-TTC TAC AAT GAG CTG CGT GTG-3′, Reverse: 5′-GGG GTG TTG AAG GTC TCA AA-3′) was used as a housekeeping gene.

The fractional cycle number at which fluorescence passed the threshold (Ct values) was used for quantification by the comparative Ct method. Sample values were normalized to the threshold value of housekeeping gene β-actin:$\Delta C_T = C_T(experiments) - C_T(\beta - \text{actin})$. The Ct value of the control (Glass substrate) was used as a reference. $\Delta\Delta C_T = \Delta C_T(experiment) - \Delta C_T(control)$. mRNA expression was calculated by the following equation: $fold\ change = 2^{-\Delta\Delta C_T}$.

5.10. In-cell Western

For evaluation of the protein levels of α_5 and α_v integrins and NaBC1 transporter, we used In-Cell Western quantification. 10.000 cells cm^{-2} of C2C12 cells were seeded onto FN-coated substrates during 1.5 h at 37 °C and 5% CO_2. Cells were then fixed using fixative buffer (10 mL) formaldehyde, 90 mL PBS, 2 g sucrose) at 37 °C for 15 min and then permeabilized in cold methanol at 40 °C for 5 min. Cells were then blocked in 0.5% blocking buffer (non-fat dry milk powder in 0.1% PBST buffer) at RT for 2 h followed by 3 washes of 10 min with 0.1% PBST. Cells were then incubated with primary antibodies: NaBC1 (abcam, 1:200), integrin α_5 (abcam, 1:500) and anti-integrin α_v (abcam, 1:500) diluted in blocking buffer at 4 °C overnight. After 3 washes of 10 min with 0.1% PBST buffer, cells were incubated with 1:800 diluted infrared-labeled secondary antibody IRDye 800CW (LI-COR) and 1:500 diluted CellTag 700 Stain (LI-COR) at RT for 1 h, followed by 5 washes of 10 min with 0.1% PBST. Samples were then dried overnight at room temperature. Infrared signal was detected using an Odyssey infrared imaging system. Four biological replicas were analyzed.

5.11. In vivo model of muscle injury

Eight-week-old male C57BL/6 mice were fed with standard diet and provided free access to water. All the experimental procedures were performed in compliance with protocols approved by the institutional animal care and use committee of the University of Basque Country UPV/EHU (Permit Number: M20/2018/145).

20 μL of 10 μM cardiotoxin (CTX) from Latoxan S.A.S. (Portes-Les-Valence, France) was administered by intramuscular injection into the right tibialis anterior muscle of anesthetized mice. After 3 days of muscle injury induction, 100 μL (equivalent to 5 mm diameter hydrogels) of alginate (ALG) and 0.59 mM borax-loaded alginate hydrogels (ALG-B) were subcutaneously injected into the right tibialis anterior muscle of anesthetized mice in the same place of the muscle lesion. Three different groups of mice were evaluated: 6 animals without implant were used as a control, 6 animals with ALG implant as a control of empty hydrogel and CTX injury, and 6 animals with ALG-B implant to observe borax effects in muscle regeneration after injury.

After 15 days post-implant, mice were sacrificed by cervical dislocation and the tibialis anterior was removed and immediately fixed in cold isopentane (−150° to −160 °C) (PanReac Applichem) for 1 min, and subsequently immersed on liquid nitrogen for 2 min. Samples were

stored at −80 °C until sectioning.

5.12. Histology and staining

Frozen tibialis anterior muscle samples were directly sectioned (without inclusion in a freezing compound), using a cryostat at −25 °C. 10 μm sections were placed on polarized slides (Superfrost, Thermofisher) and stained with Hematoxilin-eosin following standard procedures. After sample dehydration with graded ethanol series and clearing with xylene, they were mounted with xylene-based mounting medium (Entellan, Electron Microscopy Sciences). Images were captured with a bright-field microscope at 20× magnification.

For immunohistochemistry, frozen slides containing sectioned muscle samples were air-dry for 15 min at room temperature. Samples were then permeabilized with DPBS/0.5% Triton X-100 at room temperature for 5 min, next blocked in 2% BSA/DPBS for 1 h at 37 °C, and then incubated with primary antibodies in blocking solution overnight at 4 °C. The samples were then rinsed twice in DPBS/0.1% Triton X-100 and incubated with the secondary antibody at room temperature for 1 h. Finally, samples were washed twice in DPBS/0.1% Triton X-100 before mounting with Vectashield containing DAPI (Vector Laboratories) and observed under an epifluorescence microscope (Nikon Eclipse 80i).

Monoclonal primary antibodies against Laminin detection (Sigma-Aldrich, 1:30), chloride channel CLC-1 (Alpha Diagnostic, 1:400), CD31 (abcam, 1:300), fibronectin (Sigma-Aldrich, 1:400) and Alexa fluor 555 (ThermoFisher, 1:700) secondary antibody was used.

5.13. Image analysis

For focal adhesion analysis, vinculin images were segmented by ImageJ, using Trainable Weka Segmentation plugin to create a binary mask. After segmentation, focal adhesion number, size and area were determined using different commands of the same software. Values of focal adhesion size frequency were represented using GraphPad Prism 6.0. Cell morphology was analyzed by calculation of different parameters using ImageJ software. Staining intensity of immunofluorescence images were quantified by ImageJ software.

For reorganization experiments, dark individual cell areas corresponding to reorganized fibronectin deposited onto substrates by cells, were measured using ImageJ software.

For calculation of fusion index, total nuclei per image were counted from myotube images from differentiation experiments using the particle analysis command. Then, the segmented DAPI channel image was subtracted from the Cy3 channel segmented image, and the remaining nuclei were counted and assigned to non-differentiated cells. The fusion index expressed in %, was calculated subtracting the non-differentiated nuclei from the total nuclei counted. Myotubes were only considered when 3 or more nuclei were aligned inside cells.

5.14. Statistical analysis

All experiments were performed at least three times unless otherwise noted. Data were reported as mean ± standard error. To establish if our data follow a normal distribution, D'Agostino Pearson omnibus test was resorted. Results were analyzed by one-way ANOVA when 3 or more groups were compared, using GraphPad Prism 6.0. If treatment level differences were determined to be significant, multiple comparisons were performed using a Tukey in case of normal distribution of data or a Dunn's test in the contrary case. A 95% confidence level was considered significant.

Two-way ANOVA was used when comparing differences among rows and columns. Multiple comparisons were performed applying Tukey's correction when necessary.

Pairs of samples were compared using unpaired *t*-tests, applying Welch's correction when necessary. A 95% confidence level was considered significant.

Supplementary data to this article can be found online at https://doi.org/10.1016/j.msec.2021.112003.

CRediT authorship contribution statement

Jesús Ciriza: *In vivo* and hydrogel Investigation, *in vivo* and hydrogel Resources, Project administration, Writing-Review & Editing.

Ana Rodríguez-Romano: *In vivo* Investigation, *in vivo* Formal analysis, Visualization.

Ignacio Nogueroles: *In vivo* Investigation, *in vivo* Formal analysis.

Gloria Gallego-Ferrer: Hydrogel Investigation, Writing-Review & Editing.

Rubén Martín Cabezuelo: Hydrogel rheometry measurements Investigation.

José Luis Pedraz: *In vivo* and hydrogel Resources.

Patricia Rico: Conceptualization, Methodology, Validation, *in vitro* and *in vivo* Formal analysis, *in vitro* and *in vivo* Investigation, Resources, Writing-Review & Editing, Supervision, Project administration, Visualization, Funding acquisition.

Declaration of competing interest

The authors declare that they have no known competing financial interests or personal relationships that could have appeared to influence the work reported in this paper.

Acknowledgements

Funding: PR acknowledges support from the Spanish Ministry of Science, Innovation and Universities (RTI2018-096794), and Fondo Europeo de Desarrollo Regional (FEDER). CIBER-BBN is an initiative funded by the VI National R&D&I Plan 2008–2011, Iniciativa Ingenio 2010, Consolider Program, CIBER Actions and financed by the Instituto de Salud Carlos III with assistance from the European Regional Development Fund. The authors wish to thank also the intellectual and technical assistance from the ICTS 'NANBIOSIS', more specifically by the Drug Formulation Unit (U10) of the CIBER in Bioengineering, Biomaterials & Nanomedicine (CIBER-BBN) at the University of Basque Country (UPV/EHU). The authors are grateful to A. Miralles for the credit of image of the mouse included in the graphical abstract.

References

[1] Y.X. Wang, M.A. Rudnicki, Mol. Cell. Biol. 13 (2012) 127.
[2] A. Musarò, Adv. Biol. *2014* (**2014**) 1.
[3] R.C. Liddington, M.H. Ginsberg, J. Cell Biol. 158 (2002) 833.
[4] C.K. Miranti, J.S. Brugge, Nat. Cell Biol. 4 (2002) E83.
[5] D. Gullberg, T. Velling, L. Lohikangas, C.F. Tiger, Front. Biosci. 3 (1998) D1039.
[6] D. Taverna, M. H. Disatnik, H. Rayburn, R. T. Bronson, J. Yang, T. A. Rando, R. O. Hynes, J. Cell Biol.1998, *143*,849.
[7] H. Liu, A. Niu, S.-E. Chen, Y.-P. Li, FASEB J. 25 (2011) 1914.
[8] P.D. Yurchenco, Cold Spring Harb. Perspect. Biol. 3 (2011), a004911.
[9] Y.X. Wang, N.A. Dumont, M.A. Rudnicki, J. Cell Sci. 127 (2014) 4543.
[10] L. Lukjanenko, M.J. Jung, N. Hegde, C. Perruisseau-Carrier, E. Migliavacca, M. Rozo, S. Karaz, et al., Nat. Med. 22 (2016) 897.
[11] B. Hille, Ion Channels of Excitable Membranes, Sinauer Associates, Oxford, 2001.
[12] I. Lauritzen, J. Chemin, E. Honoré, J. Martine, N. Guy, M. Lazdunski, A.J. Patel, EMBO Rep. 6 (2005) 642.
[13] A.N. Gasparski, K.A. Beningo, Arch. Biochem. Biophys. 586 (2015) 20.
[14] A. Schwab, A. Fabian, P.J. Hanley, C. Stock, Physiol. Rev. 92 (2012) 1865.
[15] A. Becchetti, A. Arcangeli, Adv. Exp. Med. Biol 674 (2010) 107.
[16] M. Park, Q. Li, N. Shcheynikov, W. Zeng, S. Muallem, Mol. Cell 16 (2004) 331.
[17] E.N. Vithana, P. Morgan, P. Sundaresan, N.D. Ebenezer, D.T. Tan, M.D. Mohamed, et al., Nat. Genet. 38 (2006) 755.
[18] I.A. Lopez, M.I. Rosenblatt, C. Kim, G.C. Galbraith, S.M. Jones, L. Kao, D. Newman, W. Liu, S. Yeh, A. Pushkin, N. Abuladze, I. Kurtz, J. Biol. Chem. 284 (2009), 26882.
[19] P. Rico, A. Rodrigo-Navarro, M. Salmeron-Sanchez, Tissue Eng. A 21 (2015) 2662.
[20] P. Rico, A. Rodrigo-Navarro, M. de la Peña, V. Moulisová, M. Costell, M. Salmeron-Sanchez, Adv. Biosyst. 3 (2018), 1800220.
[21] P. Rico, A. Rodrigo-Navarro, L. Sánchez Pérez, M. Salmeron-Sanchez, Commun. Biol. 3 (2020) 717.
[22] H. Apdik, A. Dogan, S. Demirci, S. Aydin, F. Sahin, Biol. Trace Elem. Res. 165 (2015) 123.

[23] W. Yang, X. Gao, B. Wang, Med. Res. Rev. 23 (2003) 346.
[24] S. Danti, G. Ciofani, G. Pertici, S. Moscato, D. A'Alessandro, E. Ciabatti, F. Chiellini, M. D'Acunto, V. Mattoli, S. Berrettini, Tissue Eng. Regen. Med. 9 (2015) 847.
[25] P. Balasubramanian, T. Bütner, V. Miguez Pacheco, A.R. Boccaccini, J. Eur. Ceram. Soc. 38 (2018) 855.
[26] D. Kuraitis, C. Giordano, M. Ruel, A. Musarò, E.J. Suuronen, Biomaterials 33 (2012) 428.
[27] J. Liu, D. Saul, K.O. Böker, J. Ernst, W. Lehman, A.F. Schilling, Biomed. Res. Int. 2018 (2018), 1984879.
[28] K.H. Nakayama, M. Shayan, N.F. Huang, Adv. Healthc. Mater. 8 (2019), 1801168.
[29] G.D. Mulbauer, H.W.T. Matthew, Discoveries 7 (2019), e90.
[30] P. Konieczny, S. Selma-Soriano, A.S. Rapisarda, et al., Drug Discov. Today 22 (2017) 1740.
[31] W.K.M. Liew, P.B. Kang, Ther, Adv. Neurol. Dis. Ther. 6 (2013) 147.
[32] R. Chhabra, B. Ruozi, A. Vilella, et al., CNS Neurol. Disord. Drug Targets 14 (2015) 1041.
[33] T. Amna, H.M. Shamshi, M.S. Khil, et al., Surf. Interface Anal. 46 (2014) 72.
[34] M. Murariu, A. Doumbia, L. Bonnaud, et al., Biomacromolecules 12 (2011) 1762.
[35] H. Oliveira, S. Catros, C. Boiziau, et al., Acta Biomater. 29 (2016) 435.
[36] S. Burattini, R. Ferri, M. Battistelli, R. Curci, F. Luchetti, E. Falcieri, Eur. J. Histochem. 48 (2004) 223.
[37] R.O. Hynes, Cell 69 (1992) 11.
[38] G. Hofmann, P.A. Bernabei, O. Crociani, et al., J. Biol. Chem. 276 (2001) 4923.
[39] A. Becchetti, A. Arcangeli, M.R. Del Bene, et al., Proc. R. Soc. Lond. (Biol.) 248 (1992) 235.
[40] A. Arcangeli, A. Becchetti, Trends Cell Biol. 16 (2006) 631.
[41] L.A. Sabourin, M.A. Rudnicki, Clin. Genet. 57 (2000) 16.
[42] K. Tanaka, K. Sato, T. Yoshida, T. Fukuda, K. Hanamura, N. Kojima, T. Shirao, T. Yanagawa, H. Watanabe, Muscle Nerve 44 (2011) 968.
[43] N.M. McKenna, C.S. Johnson, Y.L. Wang, J. Cell Biol. 103 (1986) 2163.
[44] A. Espona-Noguera, J. Ciriza, A. Cañibano-Hernández, L. Fernández, I. Ochoa, L. Saenz del Burgo, J.L. Pedraz, Int. J. Biol. Macromol. 107 (2018) 1261.
[45] S. Poveda-Reyes, A. Rodrigo-Navarro, T.C. Gamboa-Martínez, J.C. Rodríguez-Cabello, L. Quintanilla-Sierra, U. Edlund, G. Gallego Ferrer, Polymer 74 (2015) 224.
[46] D. Hardy, A. Besnard, M. Latil, G. Jouvion, et al., PLoS ONE 11 (2016), e0147198.
[47] O. Guardiola, G. Andolfi, M. Tirone, F. Iavarone, S. Brunelli, G. Minchiotti, J. Vis. Exp. 119 (2017), e54515.
[48] R.N. Kanadia, J. Shin, Y. Yuan, S.G. Beattie, T.M. Wheeler, C.A. Thornton, M. S. Swanson, PNAS 103 (2006), 11748.
[49] A. Lesman, J. Kofer, R. Atlas, Y.J. Blinder, Z. Kam, S. Levenberg, Biomaterials 32 (2011) 7856.
[50] B.D. Walters, J.P. Stegemann, Acta Biomater. 10 (2014) 1488.
[51] A.C. Brown, T.H. Barker, Acta Biomater. 10 (2014) 1502.
[52] V. Kroehne, I. Heschel, F. Schugner, D. Lasrich, J.W. Bartsch, H. Jockusch, J. Cell. Mol. Med. 12 (2008) 1640.
[53] M.T. Wolf, K.A. Daly, J.E. Reing, S.F. Badylak, Biomaterials 33 (2012) 2916.
[54] E.M. Cronin, F.A. Turmond, R. Bassel-Duby, et al., J Biomed Mater Res B Appl Biomater 69A (2004) 373.
[55] M.E. Hoque, W.Y. San, F. Wei, et al., Tissue Eng. A 15 (2009) 3013.
[56] A.G. Guex, D.L. Birrer, G. Fortunato, H.T. Tevaearai, M.N. Giraud, Biomed. Mater. 8 (2013), 021001.
[57] K. Garg, C.L. Ward, C.R. Rathbone, B.T. Corona, Cell Tissue Res. 358 (2014) 857.
[58] B.N. Brown, J.E. Valentin, A.M. Stewart-Akers, G.P. McCabe, S.F. Badylak, Biomaterials 30 (2009) 1482.
[59] J.H. Lee, P.A. Kosinski, D.M. Kemp, Exp. Cell Res. 307 (2005) 174.
[60] M. Cerletti, S. Jurga, C.A. Witczak, et al., Cell 134 (2008) 37.
[61] C. Borselli, C.A. Cezar, D. Shvartsman, H.H. Vandenburgh, D.J. Mooney, Biomaterials 32 (2011) 8905.
[62] S.P. Frey, H. Jansen, M.J. Raschke, R.H. Mefert, S. Ochman, Clin. Orthop. Relat. Res. 470 (2012) 3607.
[63] J.M. Grasman, D.M. Do, R.L. Page, G.D. Pins, Biomaterials 72 (2015) 49.
[64] D.W. Hammers, A. Sarathy, C.B. Pham, C.T. Drinnan, R.P. Farrar, L.J. Suggs, Biotechnol. Bioeng. 109 (2012) 1051.
[65] C. Borselli, H. Storrie, F. Benesch-Lee, et al., PNAS 107 (2010) 3287.
[66] D. Shvartsman, H. Storrie-White, K. Lee, et al., Mol. Ther. 22 (2014) 1243.
[67] V.Y. Rybalko, C.B. Pham, P.L. Hsieh, et al., Biomater. Sci. 3 (2015) 1475.
[68] J.H. Hwang, I.G. Kim, S. Piao, et al., Biomaterials 34 (2013) 6037.
[69] N. Zanou, O. Schakman, P. Louis, U.T. Ruegg, A. Dietrich, L. Birnbaumer, P. Gailly, J. Biol. Chem. 287 (2012), 14524.
[70] S. Gehlert, W. Bloch, F. Suhr, Int. J. Mol. Sci. 16 (2015) 1066.
[71] M. Pusch, Hum. Mutat. 19 (2002) 423.
[72] G.M. Camerino, A. Fonzino, E. Conte, M. Bellis, A. Mele, et al., Sci. Rep. 9 (2019) 3185.
[73] F.H. Nielsen, J. Trace Elem. Exp. Med. 9 (1996) 215.
[74] K. Rochlin, A. Yu, S. Roy, M.K. Baylies, Dev. Biol. 341 (2010) 66.
[75] G.W. deHart, T. Jin, D.E. McCloskey, et al., Proc. Natl Acad. Sci. USA 105 (2008) 7188.
[76] P. Rajagopalan, W.A. Marganski, X.Q. Brown, J.Y. Wong, Biophys. J. 87 (2004) 2818.
[77] D.H. Kim, D. Wirtz, Cell Adhes. Migr. 7 (2013) 293.